CHAPTER 4

Detection and Identification of Spectral Signatures in Rainfall and Other Meteorological Variables in NE India

Chapter 4

Detection and Identification of Spectral Signatures in Rainfall and Other Meteorological Variables in NE India

Contents

4.1 Introduction

The repercussions of climate change on rainfall are known to be the alterations in the natural cycle, in terms of increase in the frequency, intensity and amount of rainfall over a region. Studies show that the spatio-temporal distribution of rainfall undergo variations because of climate change that has been accelerated in the 21st century [1-3]. The research on variability assessment in rainfall had been a burning topic of discussions since long past [4-8]. In global context, Tabony [9] performed spectral analysis of European rainfall to detect any regular periodicities. Their findings revealed that the cycles in European rainfall at periods of 2.4 years in summer and 2.1 and 5 years in the winter. Parthasarathy and Dhar [4] performed the same to estimate the dominant periodic components in rainfall time series and their association with other teleconnections

in 60 years of annual rainfall data of 31 meteorological sub-divisions of India. The power spectrum analysis showed a significant cycle in the range of 8.5-12 years, observed mainly in and around arid and semi-arid regions of Rajasthan, Central India, and extreme South Indian peninsula, whereas another cycle of 2-3.5 years was observed over Central peninsular India, and some parts of NE India. Spectral analysis performed by Bhutiyani et al. [10] on long term temperature and precipitation over north-western Himalayan (NWH) range reveals 2.2-4.3 years periodicity to be present in precipitation, indicating towards the influence of quasi- biennial oscillation (QBD) and El Niño Southern Oscillation (ENSO). It was also concluded that the sunspot cycle may be the reason for the presence of decadal periodicity (8.3-19.3 years). Similar observations were made by Narasimha and Bhattacharya [11] too. Joshi and Pandey [7] applied spectral analysis on a hundred year of rainfall data from 1901-2000 over India. The correlogram detected the presence of a fifteen- and seventeen-year cycle for the central and northwestern parts of India. The rainfall over the central India also showed the presence of a nineteen-year cycle.

Because of the various degrees of association between meteorological parameters and rainfall, it is pertinent to characterize the spectral patterns of rainfall and its probable teleconnections with different meteorological variables. Therefore, in this study spectral analyses of rainfall and other selected meteorological parameters had been carried out. The power spectral density (PSD) estimation was performed for rainfall as well as for the other meteorological parameters. Fourier based coherence analysis was used for the detection of similarity in the spectral signatures among the data series.

4.3 Methods

4.3.1 Fast-Fourier transform

An important role in the development of spectral analysis has been played by the Fast-Fourier transform (FFT) algorithm, which makes possible the rapid calculation of the periodogram for very large data sets [12]. Developed in 1965 and 1966 by Cooley and Tookey and Gentleman and Sande, the FFT computes the Discrete Fourier Transform (DFT) of a signal [12]. DFT helps in the decomposition of a time series X_t into a sum of sinusoidal components with uncorrelated random coefficients [13]. As according to Bloomfield [13], in natural world the observed data is strictly real-valued; and at the same time can also be regarded as complex numbers with zero as imaginary parts. Thus,

a pair of real-valued time series can be regarded as the real and imaginary parts of a single complex-valued time series. Now, applying Euler's formula,

$e^{ix} = cosx + isinx$ and its inverse $cosx = \frac{1}{2}\{e^{ix} + e^{-ix}\}$ and $sinx = \frac{1}{2i}\{e^{ix} + e^{-ix}\}$ shows that the function e^{ix} is intimately related to cosines and sines.

Then, for any *n* complex numbers $x_0, x_1, \ldots, x_{n-1}$

$$d(f) = \frac{1}{n}\sum_{t=0}^{n-1} x_t\, e^{-2\pi i f t} \quad \text{……(1)}$$

where x_t is a time series and can be expressed as,

$$x_t = \sum_j d\,(f) e^{2\pi i f_j t} \quad \text{……(2)}$$

Here, $j = 0, 1, \ldots, n\text{-}1$ or $-n/2 < j \leq n/2$

The *d(f)* in equations (1) and (2) is called the DFT of the set of complex numbers $\{x_0, x_1, \ldots, x_{n-1}\}$, which are obtained from *d(f)* itself by the inverse transform in equation (2).

Two representations are used to describe DFT: (a) in terms of its real and imaginary parts as described before and (b) in terms of its magnitude $R(f) = |d(f)|$ and phase $\phi(f) = R(f)e^{i\,\phi\,(f)}$

This magnitude is the measure of the strength of the oscillation with frequency *f* and can be represented in the form $I(f) = nR(f)^2 = n|d(f)|^2$,

where *I(f)* is called the periodogram.

4.3.1 Power Spectral Density estimation

The FFT helps in the decomposition of a time series X_t into a sum of sinusoidal components with uncorrelated random coefficients. Summation or integration of the spectral components yields the total power or variance of the signal. As in the time domain the energy density is the power, for a signal existing over all time, the energy distribution in terms of frequency (per unit time) is referred to as the power spectral density, $S_{xx}(f)$ of that signal [14-15] and it specifies the frequency decomposition of the autocovariance function (ACVF) [16]. Thus, the energy of a signal is

$$E = \int_{-\infty}^{\infty} |\hat{x}(t)|^2 dt \text{ [14] [12]},$$

Where, $\hat{x} = \int_{-\infty}^{\infty} e^{-2\pi i f t} x(t) dt \hat{x} = \sum_{n=0}^{N-1} x[t].\cos(2\pi f t) - \sin(2\pi f t i)$

and is the Fourier transform of the signal, therefore power spectral density of a signal is defined as $S_{xx}(f) = |\hat{x}(f)|^2$[14][12][15].

4.3.2 Coherence

Squared Coherency (SC), or simply, coherency is a dimensionless quantity, defined as the ratio between the squared cross spectra, $|S_{xy}(f)|^2$ and the multiples of autocovariance spectra $S_{xx}(f)$ and $S_{yy}(f)$ for two signals x_t and y_t respectively. Thus, according to Brockwell and Davis [12] and Bloomfield [13], coherency is defined as

$$|C_{xy}(f)|^2 = C_{xy}(f) = \frac{|S_{xy}(f)|^2}{S_{xx}(f) \cdot S_{yy}(f)}$$

The value of coherency such computed lies in between zero and one. It can be used as a measure of dependence for multivariate time series; 0 corresponding to no dependence and 1 corresponding to a linear dependence of one variable of interest on the other at frequency *f* cycles per unit time. The values towards 0 thus signifies weaker association whereas stronger association is described by the values as they approach towards one. In this study the coherence range is set between two parameters: the coherence is weak if 0<SC>0.4, moderate if 0.4<SC>0.6 and strong if 0.6<SC>1.

The 49 years monthly average data were subjected to spectral analysis using Fast Fourier Transform (FFT) that computes the Discrete Fourier Transform (DFT) of a sequence.

4.3.3 The phase-coherence association

Spectral densities of the univariate processes *x* and *y* are the two diagonal elements of *f:*

$f_{xx}(\omega) = \frac{1}{2\pi}\sum_{j=-\infty}^{\infty} \gamma_{xx}(j)e^{-i\omega\, j}$ and $f_{yy}(\omega) = \frac{1}{2\pi}\sum_{j=-\infty}^{\infty} \gamma_{yy}(j)e^{-i\omega\, j}$

The function $f_{xy}(\omega) = \frac{1}{2\pi}\sum_{j=-\infty}^{\infty} e^{-i\omega\, j}\gamma_{xy}(j)$ is called the cross spectral density of *x* and *y*.

The cross spectrum f_{xy} can be expressed in terms of its polar coordinates as-

$$f_{xy}(\omega) = R_{xy}(\omega)e^{i\emptyset_{xy}(\omega)}$$

The real function $R_{xy}(\omega)$ is called the amplitude spectrum and $f_{xy}(\omega)$ is called the phase spectrum. $R_{xy}(\omega)$ measures the strength of the linear association of *x* and *y* at different frequencies. The squared coherency can be derived using these two functions such that

$$C_{xy}(\omega) = \frac{|f_{xy}(\omega)|^2}{f_{xx}(\omega) \cdot f_{yy}(\omega)}$$

4.4 Results and discussions

4.4.1 Power spectral density estimation

Rainfall

As evident from Figure 4.1 (a-e), the monthly rainfall time series exhibited strong annual periodicity (12 months) in the periodogram across all the selected locations of NER. The strength of the annual periodicity was the highest at CHR. A relatively weaker half annual periodicity was also evident in case of CHR and DBR.

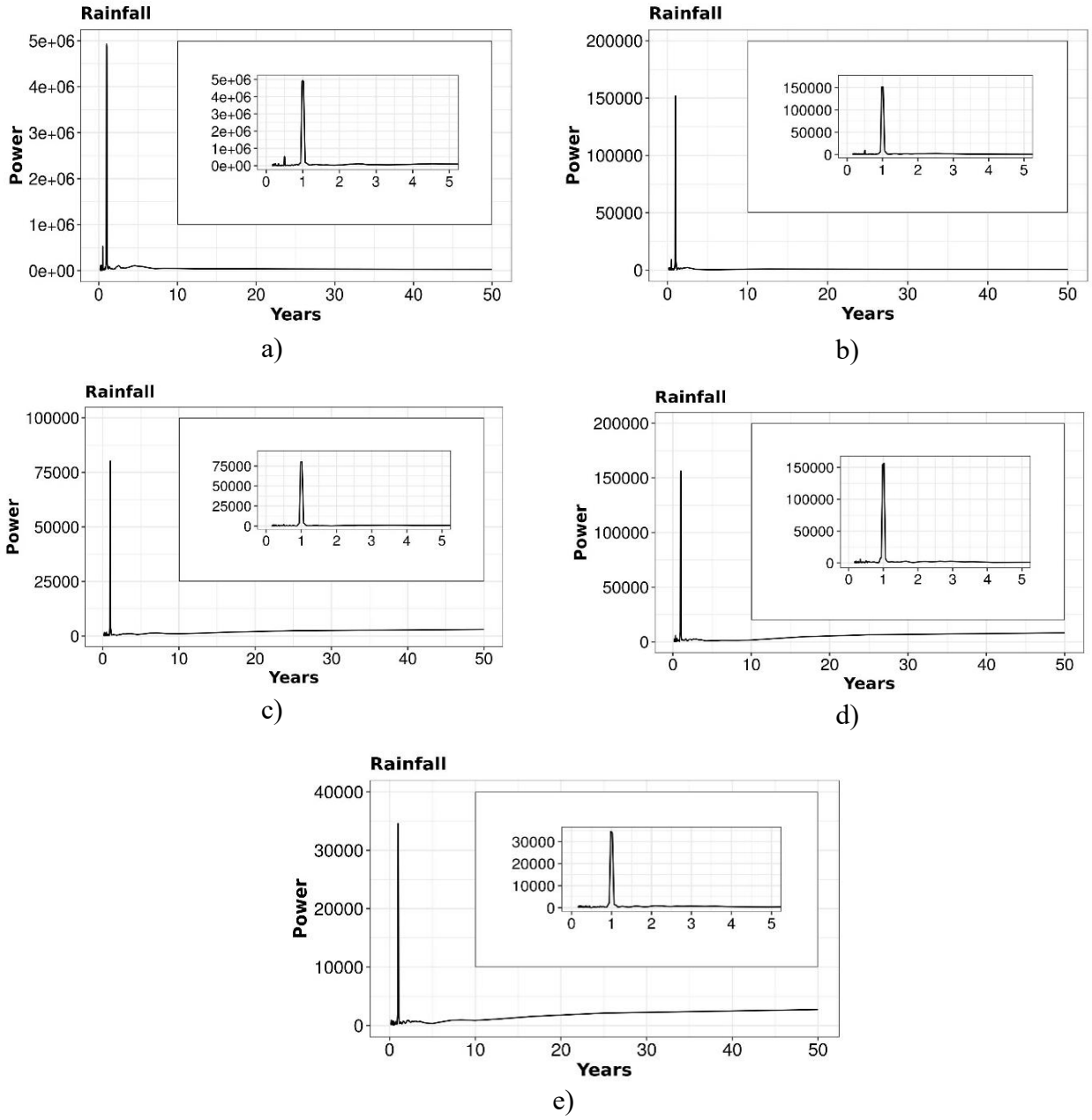

Figure 4. 1 Periodogram showing the power spectra of rainfall at a) CHR, b) DBR, c) GHY, d) KSH and e) TUL

MaxT and MinT

A strong annual periodicity was also evident in the power spectra of both MaxT and MinT (Figure 4.2 and 4.3 respectively). The order of strength of the annual cycle in MaxT is DBR>GHY>TUL>CHR>KSH, whereas in case of MinT it is TUL>DBR>GHY>KSH>CHR. In case of temperature also, another periodic signature of six months was evident across all the selected study areas. However, the strength of the half yearly period was lower in MinT as compared to that of MaxT.

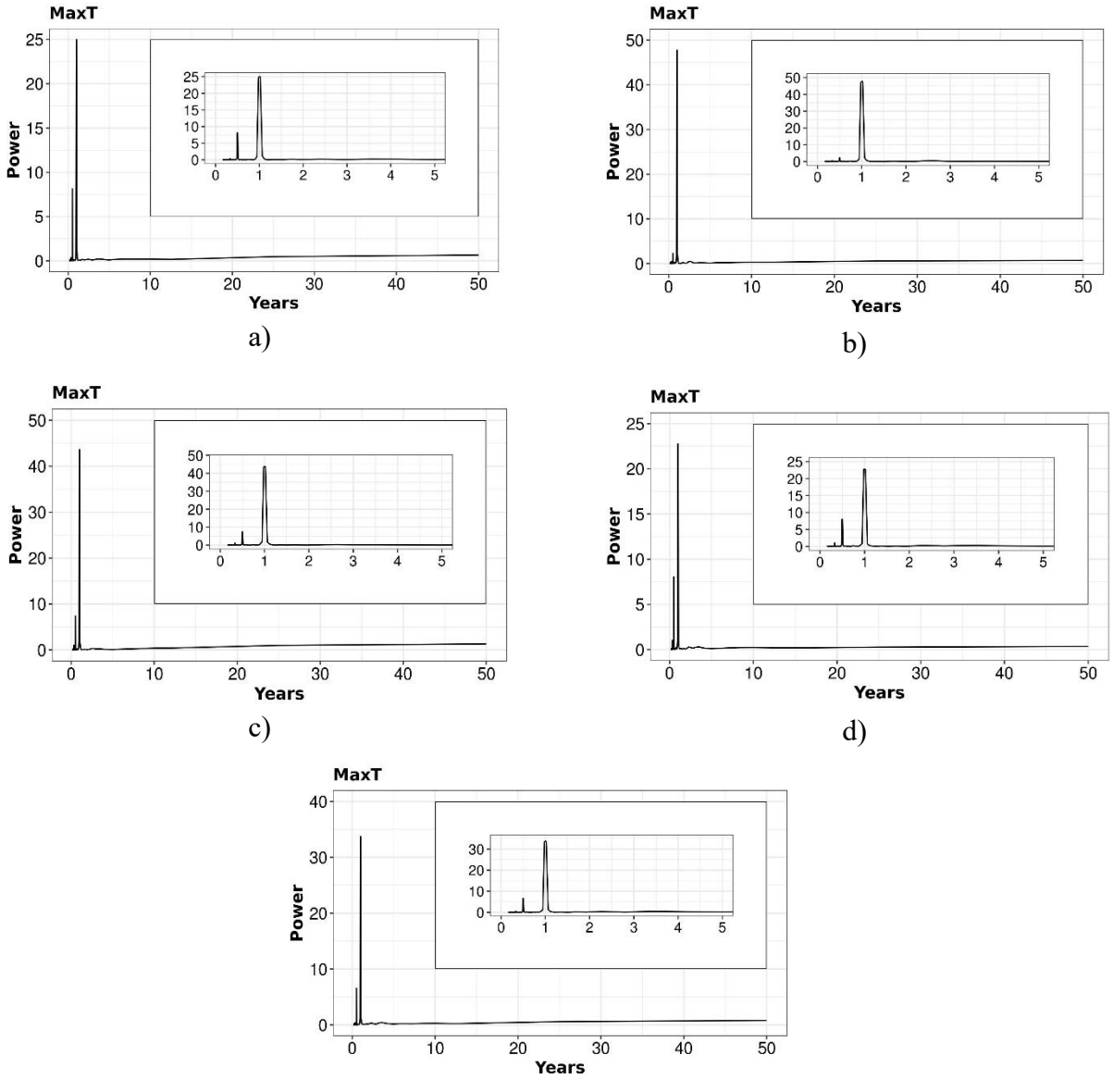

Figure 4. 2 Periodogram showing the power spectra of MaxT at a) CHR, b) DBR, c) GHY, d) KSH and e) TUL

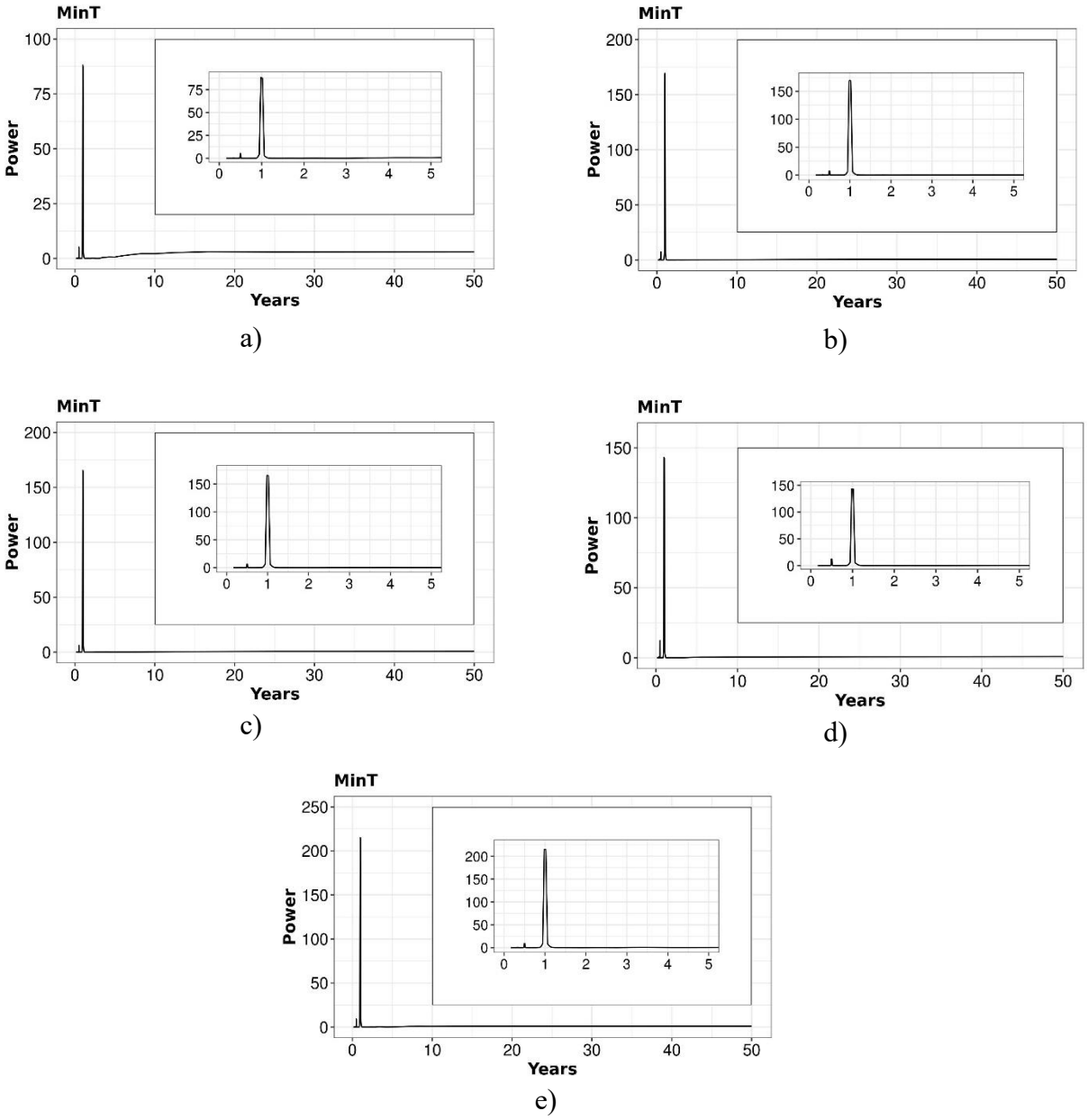

Figure 4. 3 Periodogram showing the power spectra of MinT at a) CHR, b) DBR, c) GHY, d) KSH and e) TUL

RH

All the selected study areas of NER exhibited annual and half yearly periodicities in the periodograms of RH (Figure 4.4) except for CHR (only annual periodicity was evident). Apart from them, relatively smaller peaks were evident in the power spectra of RH over NER, at 2-4 months period. The annual periodicity at CHR had the highest power followed by TUL, whereas in case of the half yearly periodicity maximum power was observed at GHY.

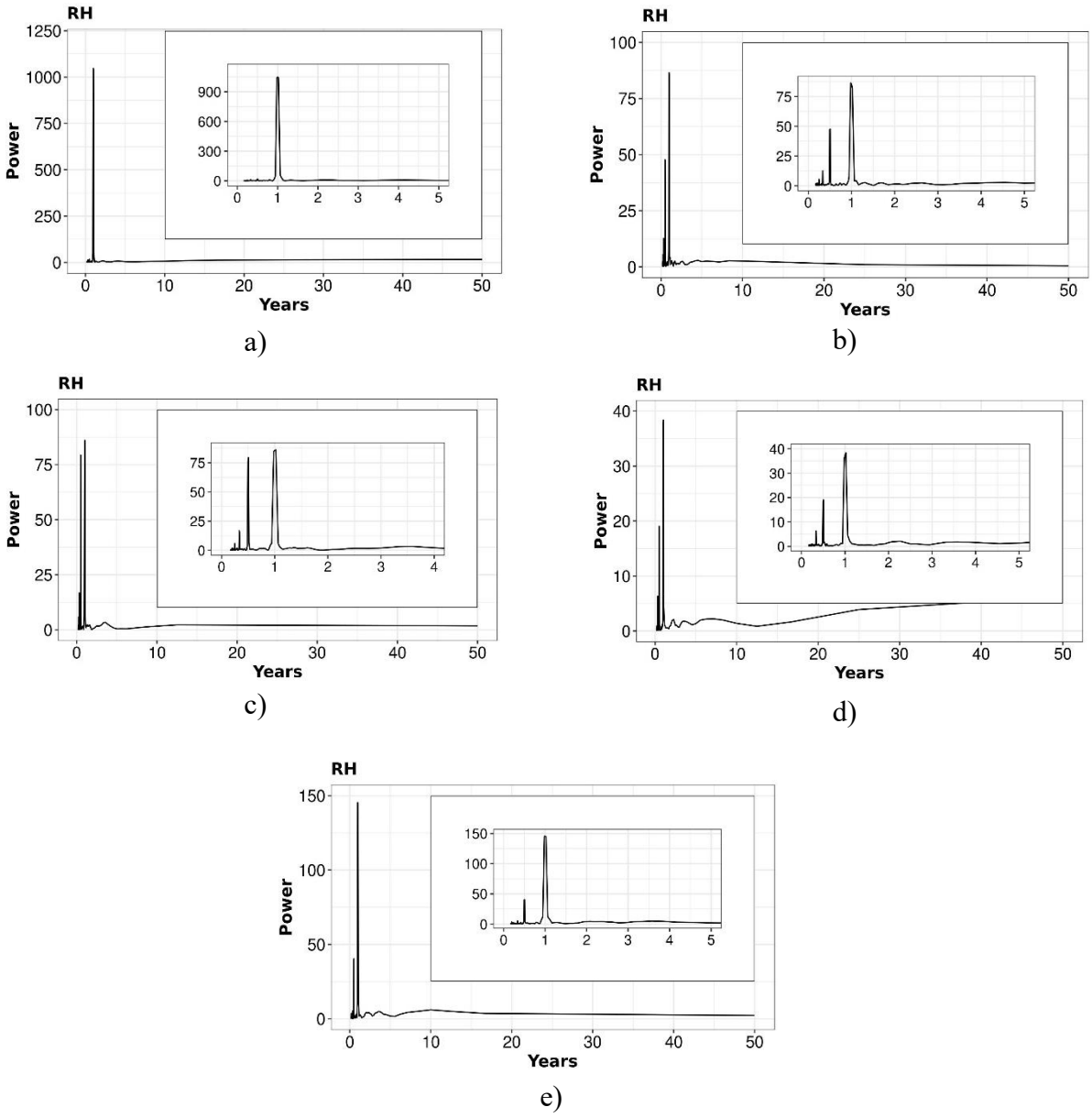

Figure 4. 4 Periodogram showing the power spectra of RH at a) CHR, b) DBR, c) GHY, d) KSH and e) TUL

SLP

The periodogram of SLP over the selected study areas (Figure 4.5) resembles similarity in the structure to the same for rainfall, with varied degree of powers in comparison.

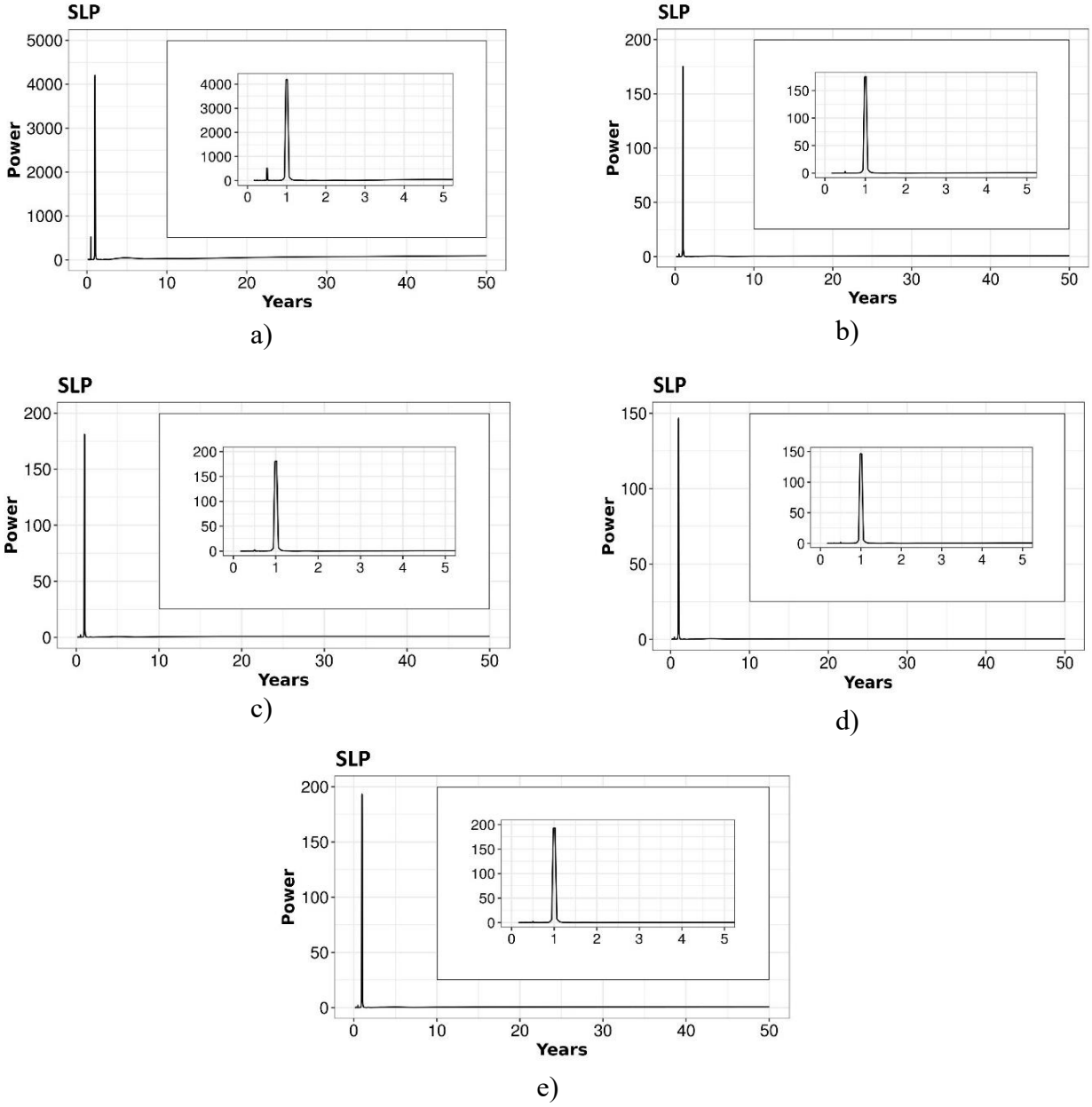

Figure 4. 5 Periodogram showing the power spectra of SLP at a) CHR, b) DBR, c) GHY, d) KSH and e) TUL

WS

The power spectra of WS at different study areas of NER (Figure 4.6) revealed an increasing pattern towards the low frequency regions. Annual and the half yearly periodicity were clear in the power spectra of WS at DBR, GHY, KSH and TUL.

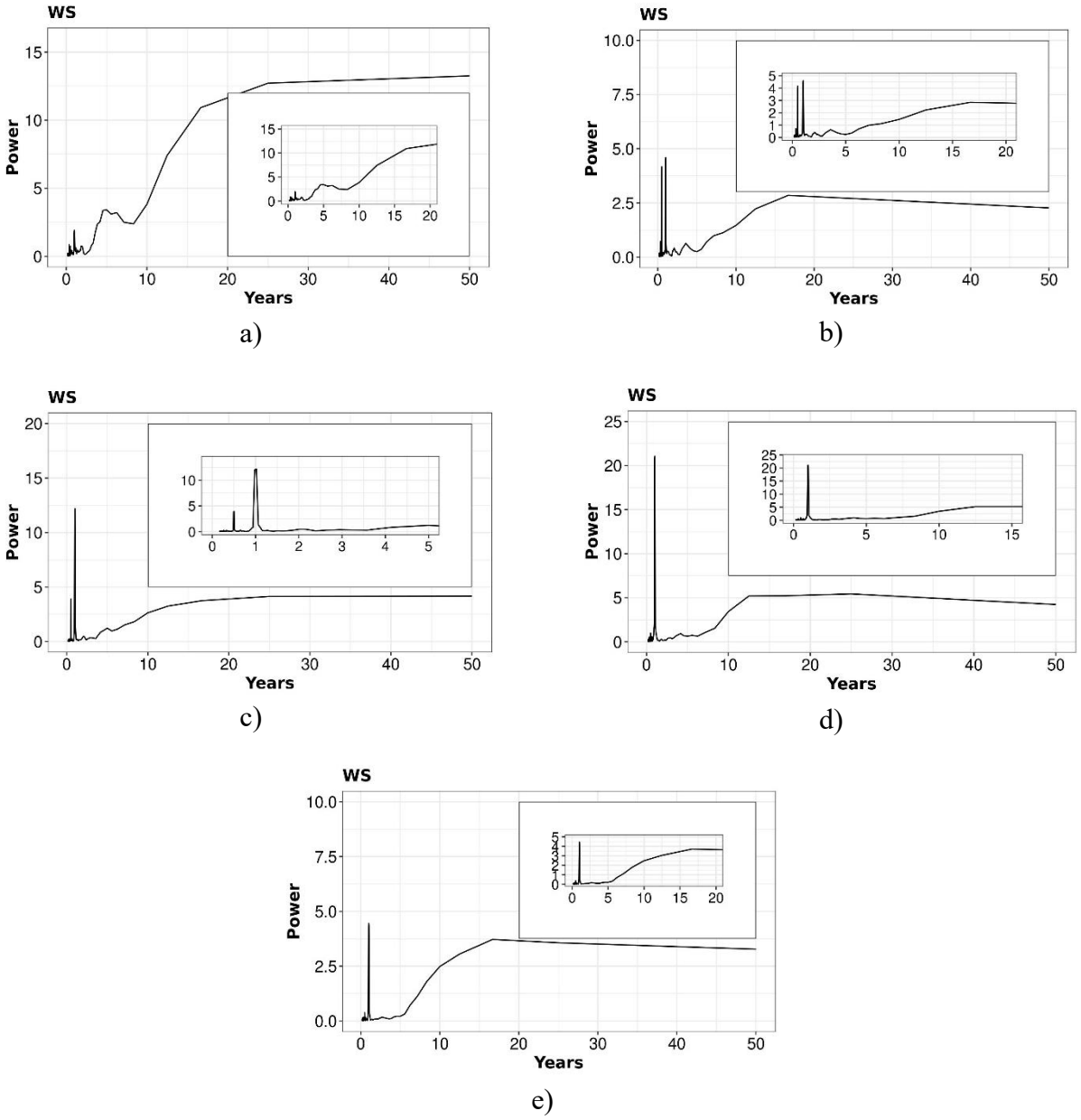

Figure 4. 6 Periodogram showing the power spectra of WS at a) CHR, b) DBR, c) GHY, d) KSH and e) TUL

4.4.2 Coherence

Rainfall and MaxT

Figure 4.7 presented the correlogram of rainfall and MaxT at different study areas. It could be seen that a strong coherence was present between these two variables in the annual periodicity. Numerous sharp peaks were observed in the high frequency region of the correlogram, while the power in the low frequency regions form an increasing trend like pattern. Moderate coherence was observed in a periodicity of 2 years in case of CHR, 2-4 years in KSH, 2.1 years in TUL.

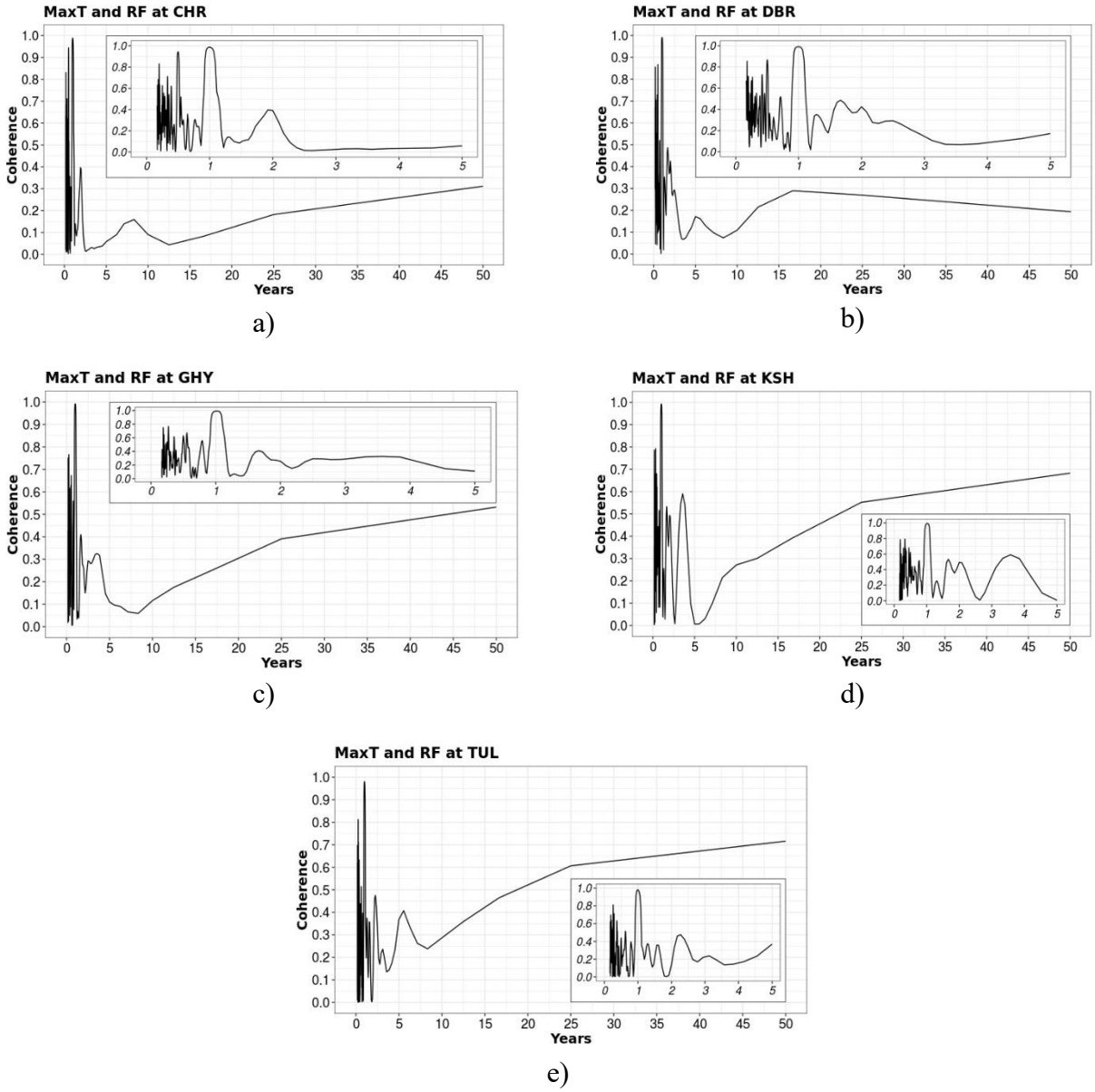

Figure 4. 7 Correlogram showing the coherence of rainfall with MaxT at a) CHR, b) DBR, c) GHY, d) KSH and e) TUL

Rainfall and MinT

In case of rainfall and MinT also, the annual period displayed a strong coherence across all the sites (Figure 4.8). Inter-annual periodicities of 2.5 years and 2-4 years were also noticed in the coherence plots, however, the strength of the association of rainfall and MinT at these periods was low (CHR, DBR) to moderate (GHY). Apert from these, many sharp peaks were noticed in between 1-6 months period.

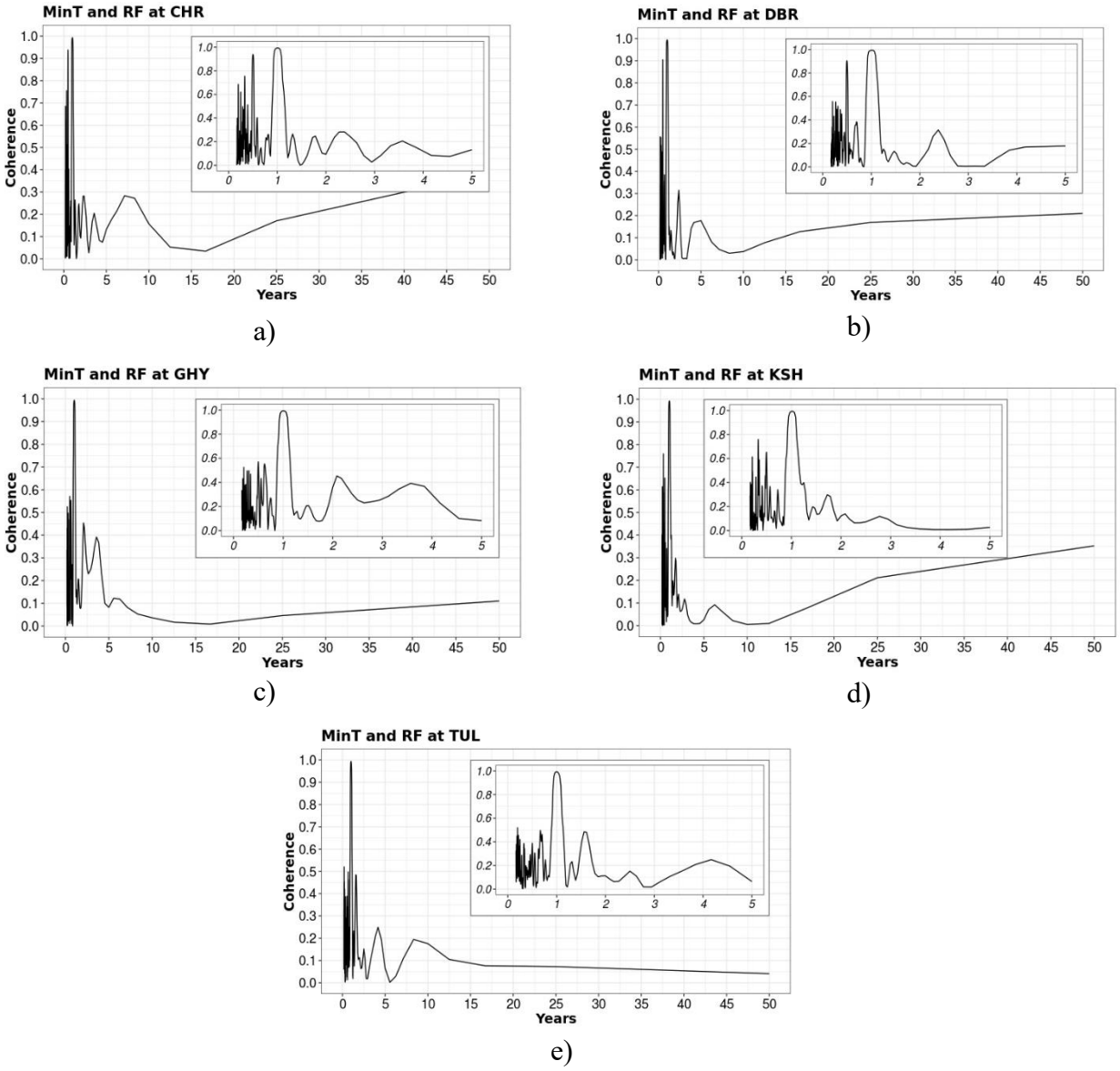

Figure 4. 8 Correlogram showing the coherence of rainfall with MinT at a) CHR, b) DBR, c) GHY, d) KSH and e) TUL

Rainfall and RH

As evident in Figure 4.9, rainfall and RH also displayed strong coherence at 1 year-period across all the selected study areas of NER. The correlograms reveal the presence of moderate coherence in the period of 3 years at CHR, 2 years at DBR and KSH, 1-2 years at GHY and 2.5 years at TUL.

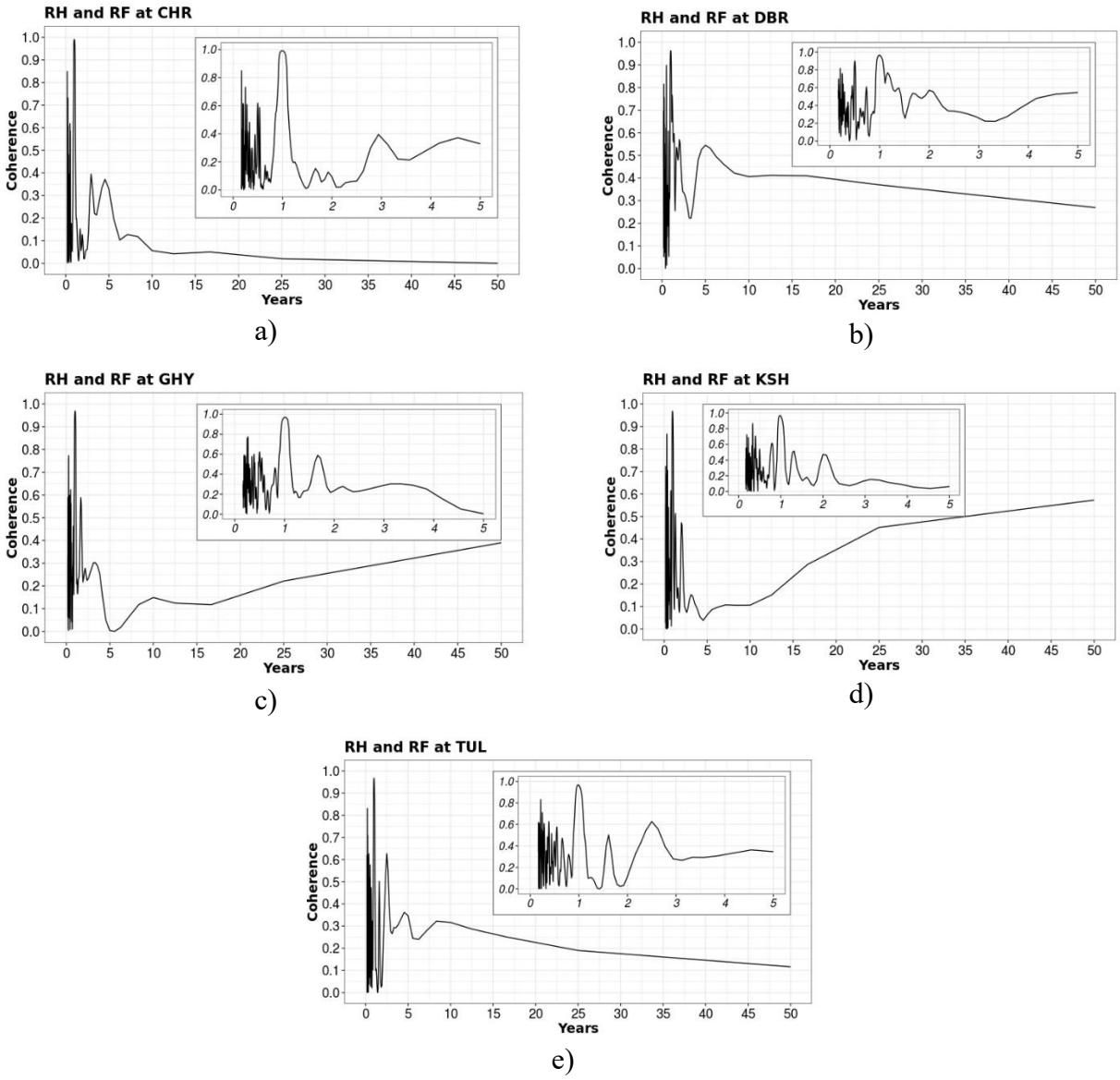

Figure 4. 9 Correlogram showing the coherence of rainfall with RH at a) CHR, b) DBR, c) GHY, d) KSH and e) TUL

Rainfall and SLP

An annual periodicity of strong coherence was evident in the correlogram of rainfall and SLP also (Figure 4.10). Another strong coherence was detected in the 4 years periodicity in case of CHR. CHR also displayed the presence of moderate coherence in 1.8 years period. On the other hand, moderate coherence was detected in 8-9 years period in case of DBR.

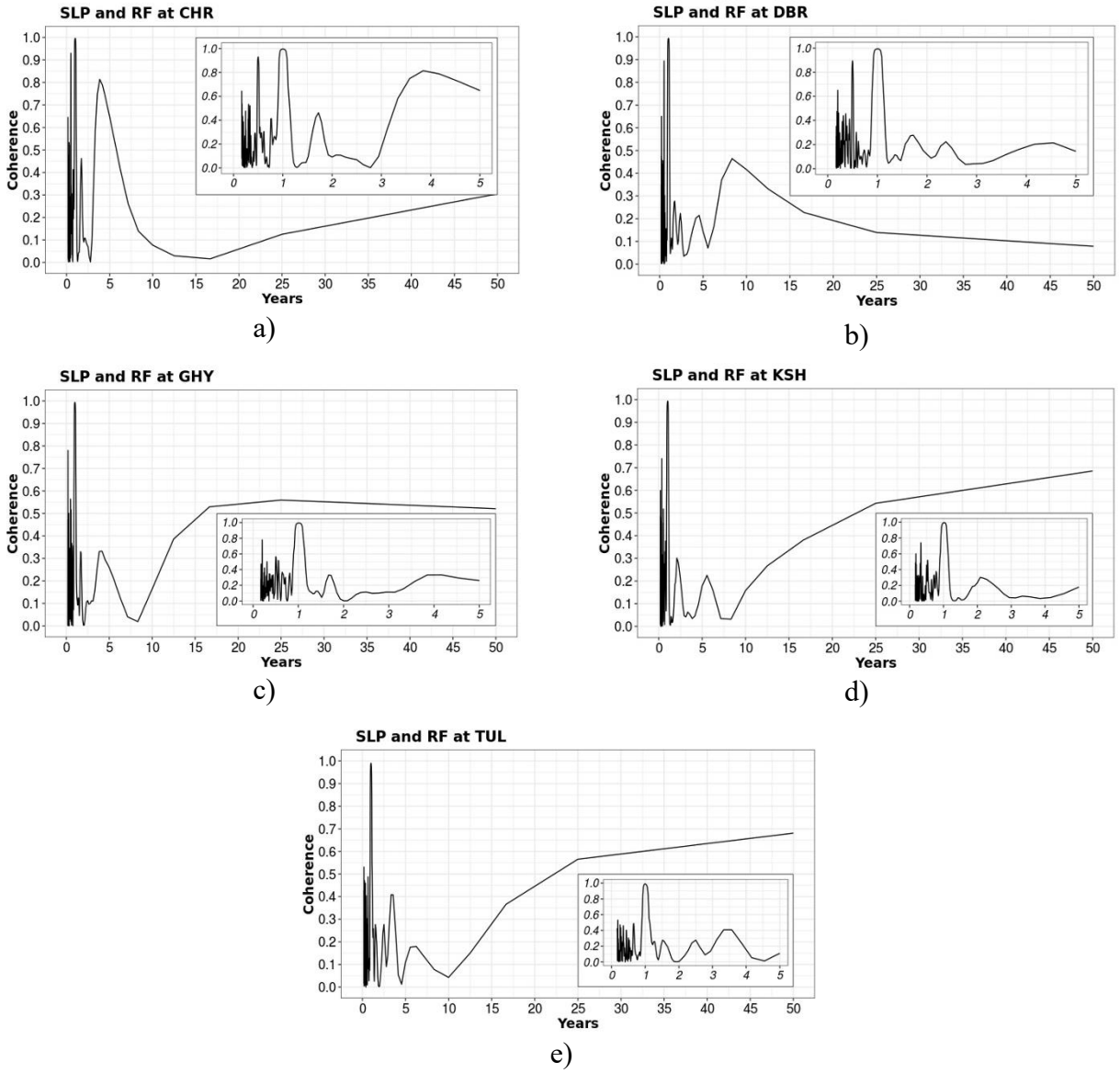

Figure 4. 10 Correlogram showing the coherence of rainfall with SLP at a) CHR, b) DBR, c) GHY, d) KSH and e) TUL

Rainfall and WS

In case of coherence between rainfall and WS also, strong association was observed in the 1-year period at all the study areas. Moderate coherence was observed in the period of 2 years at DBR, 2-3 years at KSH and TUL. The six months- period at DBR and KSH also displayed strong coherence as evident in the correlogram (Figure 4.11).

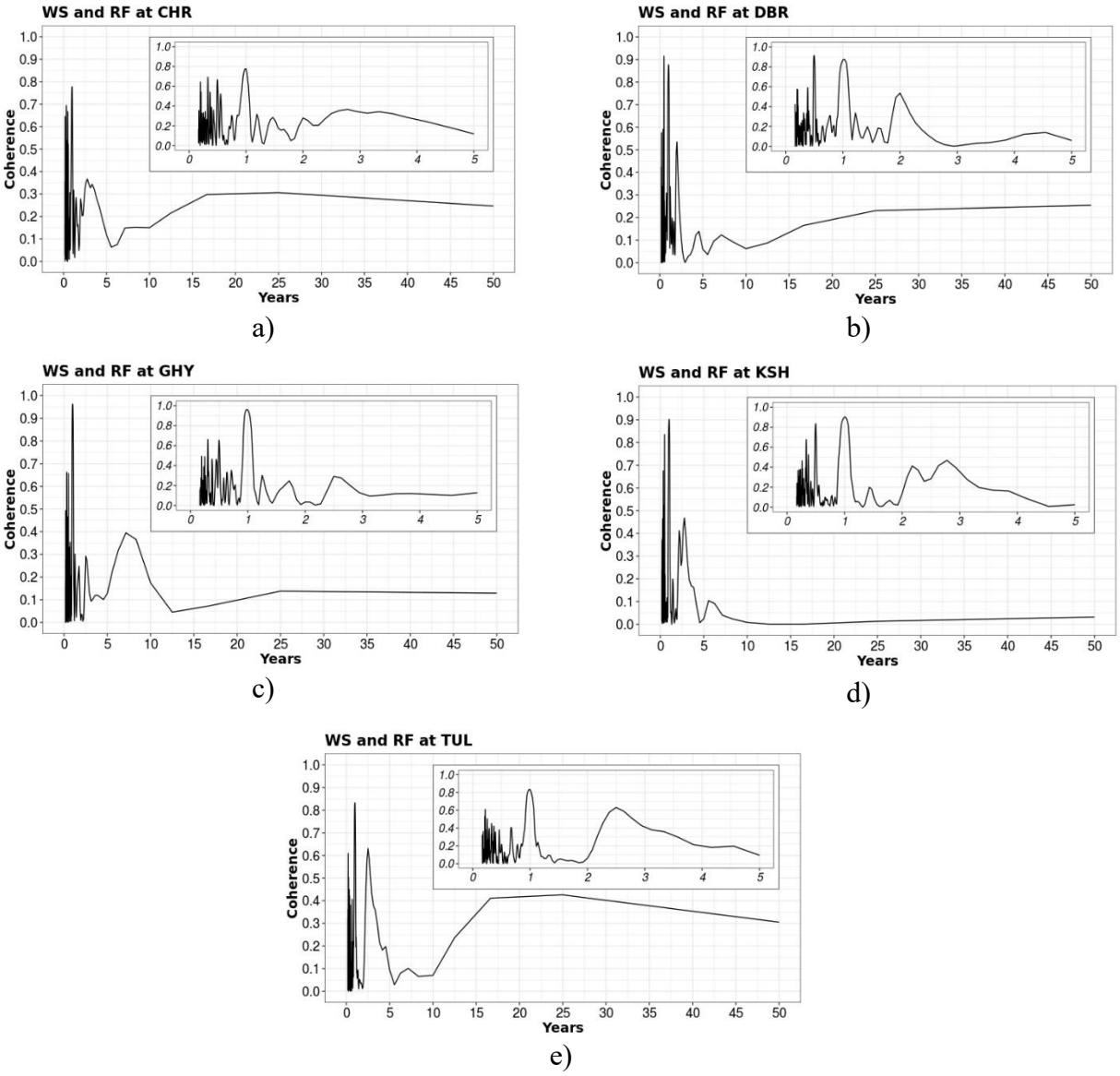

Figure 4. 11 Correlogram showing the coherence of rainfall with WS at a) CHR, b) DBR, c) GHY, d) KSH and e) TUL

4.4.3 Phase-coherence association in different meteorological variables in NER

The phase and coherence spectra for association of rainfall with different meteorological variables throughout the study areas are presented in Figure 4.12- 4.16. In these plots the primary and secondary vertical axis represents phase and coherence values respectively, while the horizontal axis represents time period in years. No definite common pattern in the phase plots could be derived from the phase plot. The

periods showing strong coherence in the phase-coherence plots seemed to be out of phase in most of the associations except the association of rainfall and SLP at KSH.

Rainfall and MaxT

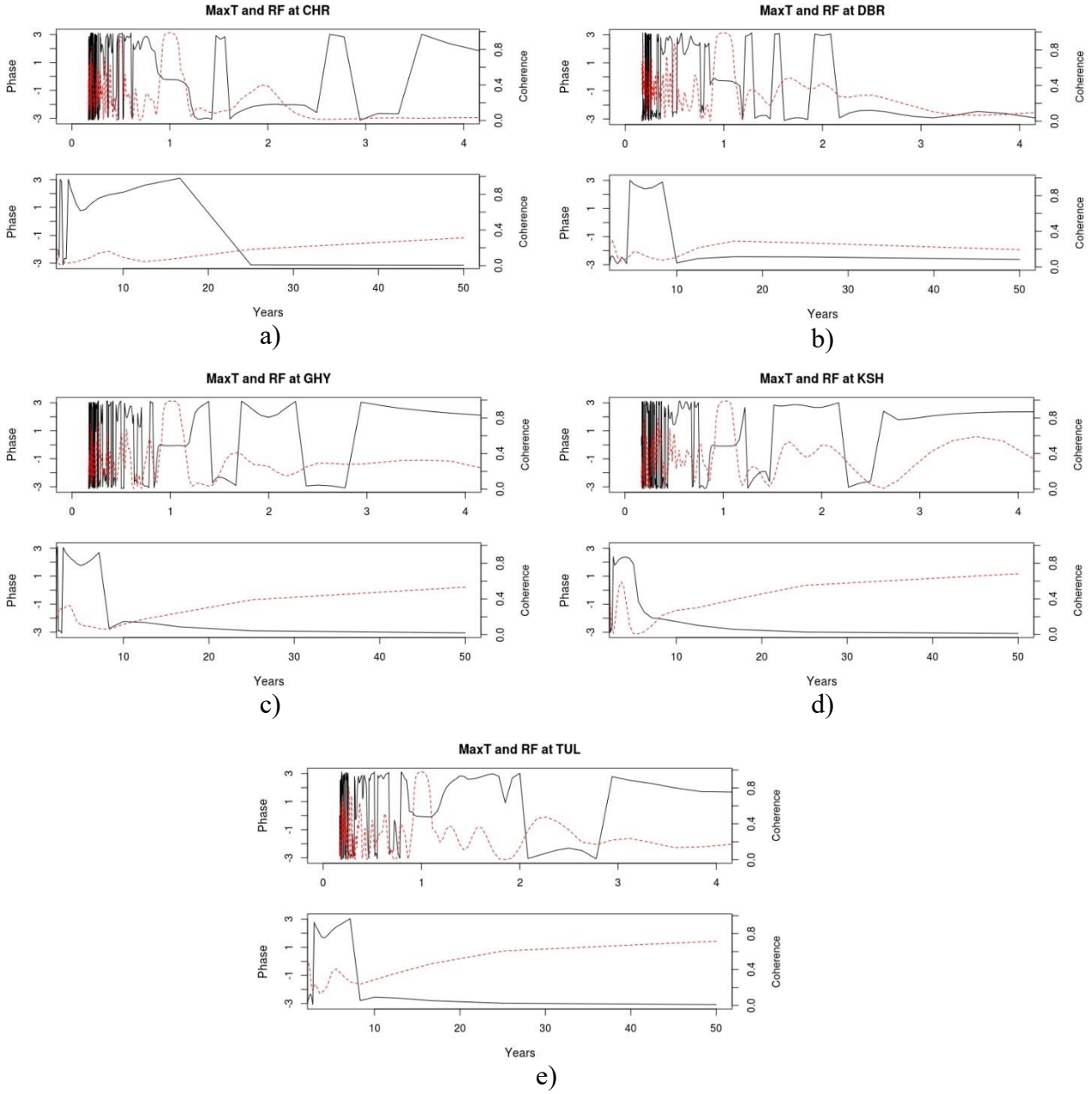

Figure 4. 12 Phase and coherence spectra of rainfall with MaxT at a) CHR, b) DBR, c) GHY, d) KSH and e) TUL; here the solid black line represents the phase spectra whereas the red dotted line represents the coherence spectra of rainfall with MaxT

Rainfall and MinT

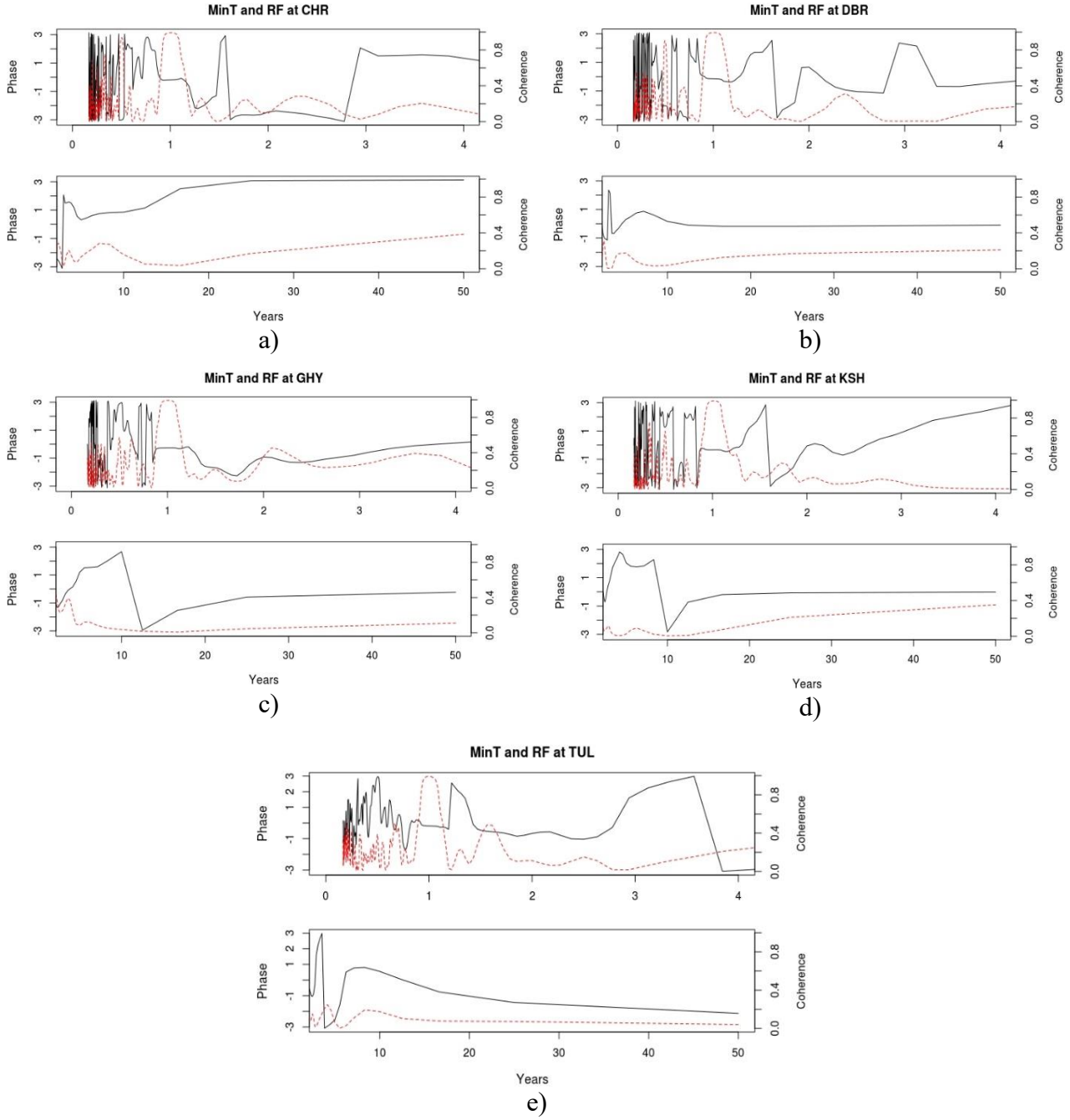

Figure 4. 13 Phase and coherence spectra of rainfall with MinT at a) CHR, b) DBR, c) GHY, d) KSH and e) TUL; here the solid black line represents the phase spectra whereas the red dotted line represents the coherence spectra of rainfall with MinT

Rainfall and RH

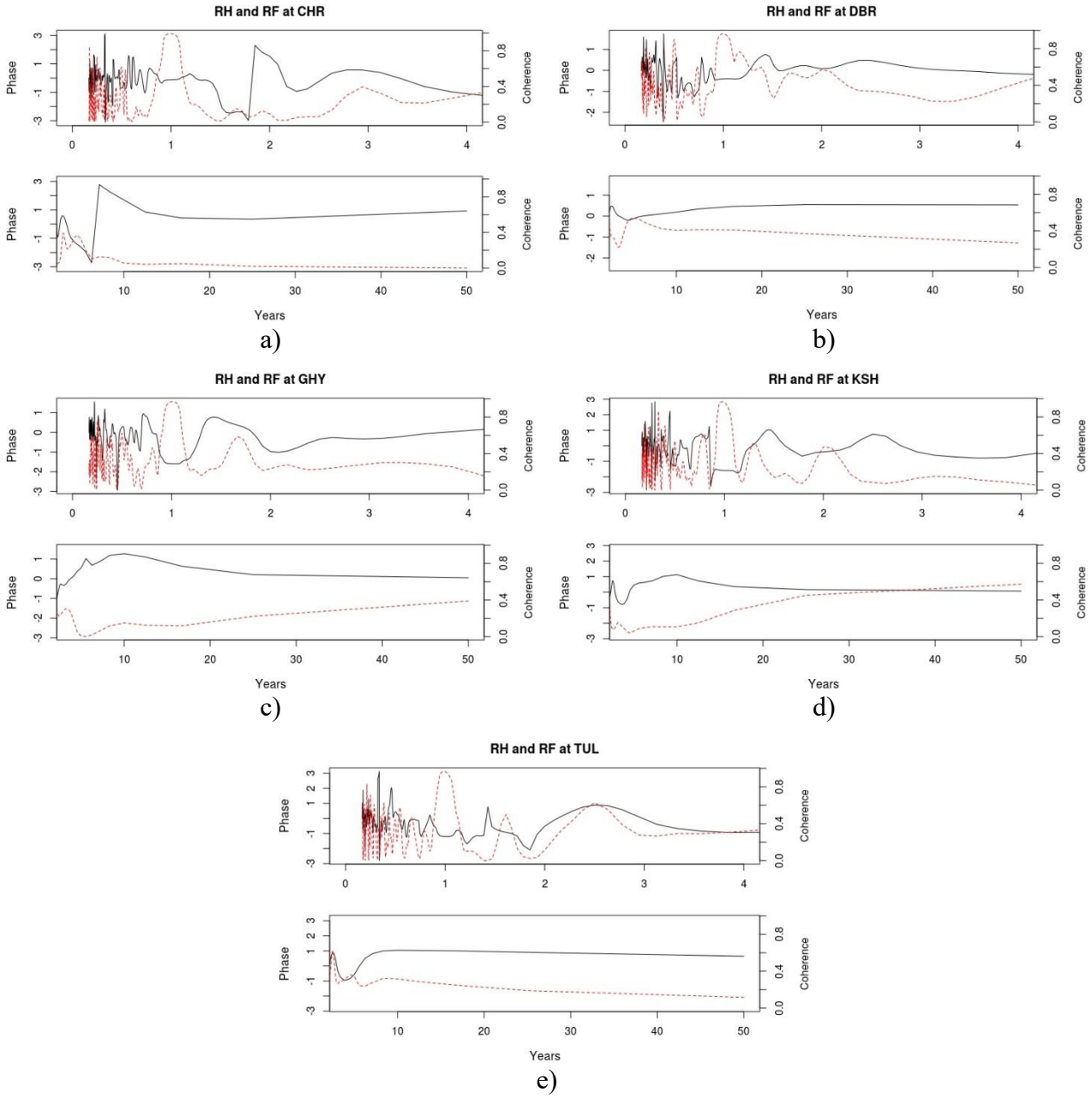

Figure 4. 14 Phase and coherence spectra of rainfall with RH at a) CHR, b) DBR, c) GHY, d) KSH and e) TUL; here the solid black line represents the phase spectra whereas the red dotted line represents the coherence spectra of rainfall with RH

Rainfall and SLP

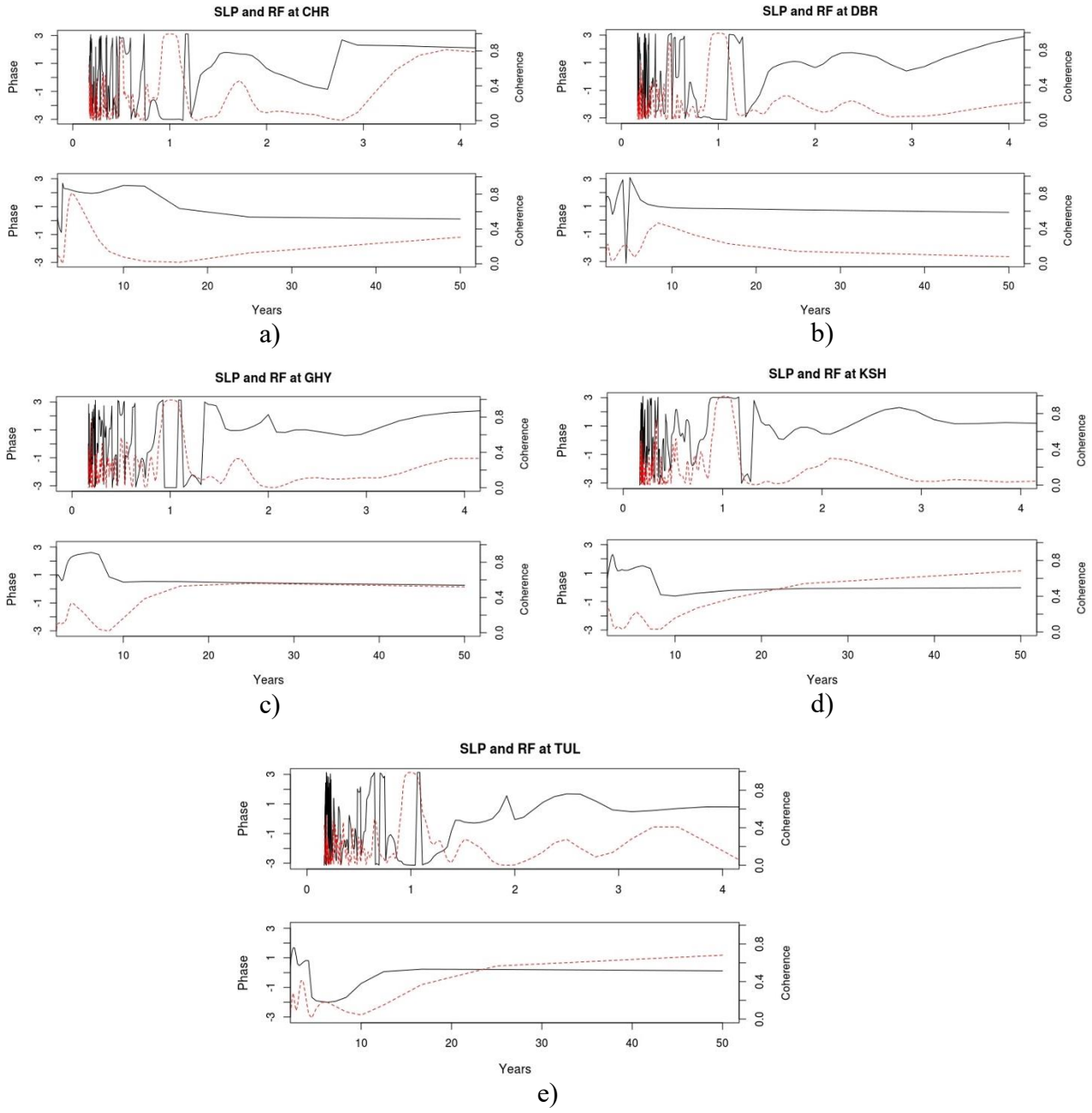

Figure 4. 15 Phase and coherence spectra of rainfall with SLP at a) CHR, b) DBR, c) GHY, d) KSH and e) TUL; here the solid black line represents the phase spectra whereas the red dotted line represents the coherence spectra of rainfall with SLP

Rainfall and WS

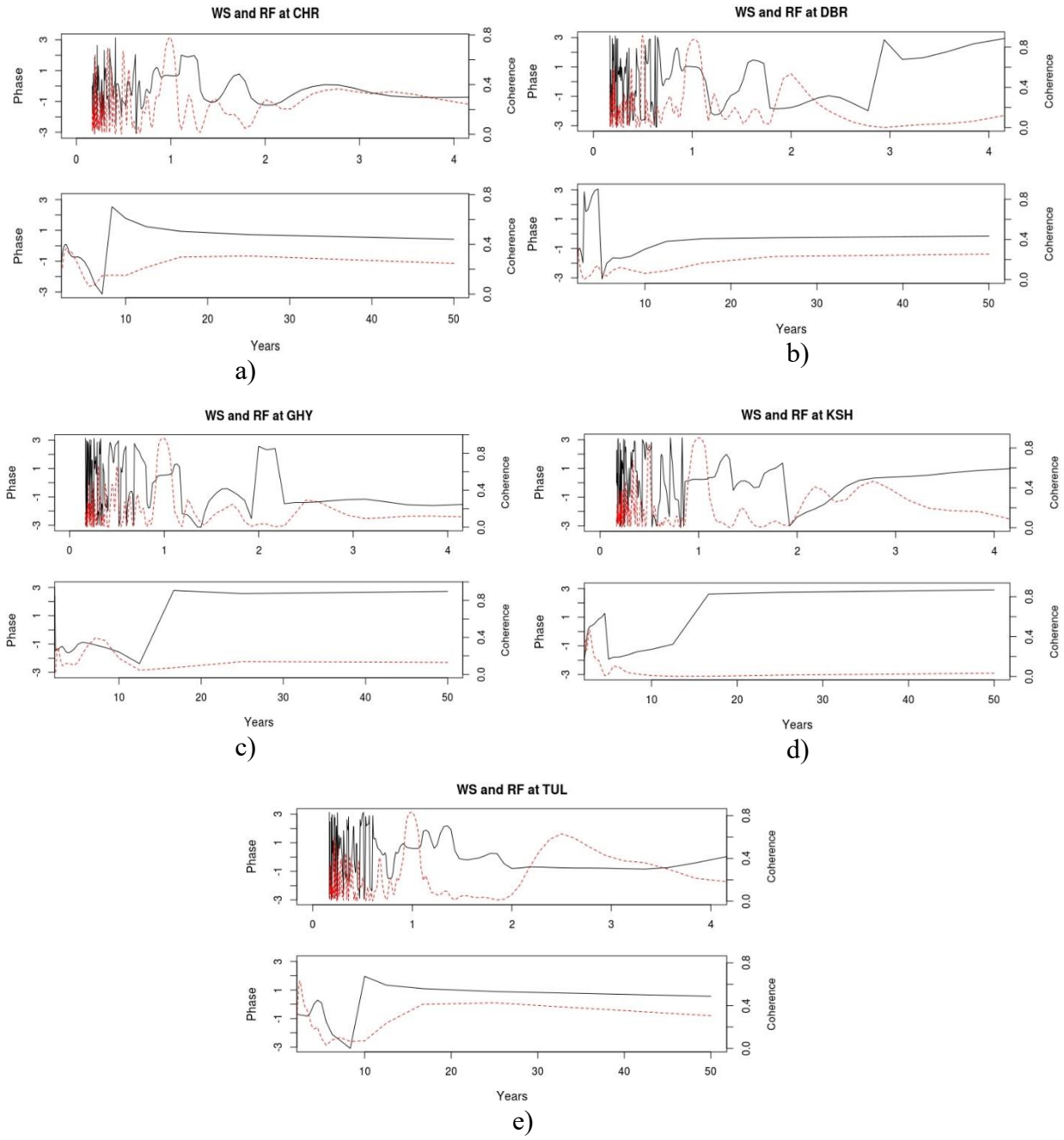

Figure 4. 16 Phase and coherence spectra of rainfall with WS at a) CHR, b) DBR, c) GHY, d) KSH and e) TUL; here the solid black line represents the phase spectra whereas the red dotted line represents the coherence spectra of rainfall with WS

4.5 Summary

Spectral analysis provides techniques in understanding the features of a time series in frequency domain, that otherwise could not be resolved in time domain. In this chapter an attempt was made to detect the spectral features or signatures in the meteorological series of rainfall, MaxT, MinT, RH, SLP and WS over selected regions in NER with the help of FFT. The PSD plots of all the meteorological variables displayed the presence of an annual periodicity. Another six months periodic component was also evident in the periodogram of most of the meteorological variables across the selected studied regions. In case of the power spectra of RH distinct peaks were observed between the periods of 2-4 months, although the power of the peaks was relatively weaker than the annual periodicity. From the coherence plots it could be seen that rainfall with the other meteorological parameters exhibited strong coherence at an annual periodicity. Another strong coherence of 4 years periodicity was observed in case of the association with SLP also (at CHR). Moderate coherence was also evident in some of the associations over certain study areas in the periodicity of 1.8 years, and in between 2-4 years periodicity as a common feature in all the associations over certain study areas. Anti-phase association could be seen in case of the annual periodicity of strong coherence throughout the considered pairs of association as evident from the phase-coherence spectra. However, leading and lagging variable association were not very evident from these plots, therefore, wavelet analyses were carried out (in Chapter 5) to have a clear insight regarding the leading-lagging association in the rainfall and other selected meteorological variables.

4.6 References

[1] Stocker, T. F., Qin, D., Plattner, G.-K., Tignor, M., Allen, S.K., Boschung, J., Nauels, A., Xia, Y., Bex, V. and Midgley, P.M. (eds.) Summary for Policymakers. In: Climate Change 2013: The Physical Science Basis. Contribution of Working Group I to the Fifth Assessment Report of the Intergovernmental Panel on Climate Change, Cambridge University Press, Cambridge, 2013.

[2] Field, C.B., Barros, V.R., Dokken, D.J., Mach, K.J., Mastrandrea, M.D., Bilir, T.E., Chatterjee, M., Ebi, K.L., Estrada, Y.O., Genova, R.C., Girma, B., Kissel, E.S., Levy, A.N., MacCracken, S, Mastrandrea, P.R. and White, L.L. (eds.) Climate Change 2014: Impacts, Adaptation, and Vulnerability. Technical report WGIIAR5, IPCC, 2014.

[3] Naidu, C.V., Rao, B.R.S. and Rao, D.V.B. Climatic trends and periodicities of annual rainfall over India. *Meteorological Applications*, 6, 395–404, 1999.

[4] Parthasarathy, B. and Dhar, O.N. Secular Variations of regional rainfall over India. *Quarterly Journal of the Royal Meteorological Society*, 100:245-257, 1974.

[5] Mooley, D. and Parthasarathy, B. Fluctuations in all-India Summer Monsoon rainfall during 1871–1978, *Climatological Change*, 6, 287–301, 1984. DOI:10.1007/BF00142477.

[6] Wu, R., and Wang, B. A. Contrast of the East Asian Summer Monsoon and ENSO relationship between 1962–1977 and 1978–1993, *Journal of Climatology*, 15, 3266–3279, 2002. DOI:10.1175/1520-0442(2002)0152.0.CO;2.

[7] Joshi, M.K. and Pandey, A.C. Trend and spectral analysis of rainfall over India during 1901–2000. *Journal of Geophysical Research,* 116:1-13, 2011. DOI:10.1029/2010JD014966.

[8] Anandharuban, P. and Elango, L. Spatio-temporal analysis of rainfall, meteorological drought and response from a water supply reservoir in the megacity of Chennai, India. *Journal of Earth System and Science*, 130(17):1-20, 2021. DOI: https://doi.org/10.1007/s12040-020-01538-2.

[9] Tabony, R.C. A principal component and spectral analysis of European rainfall. International *Journal of Climatology*, 1:283-294, 1981.

[10] Bhutiyani, M. R., Kale, V. S. and Pawar, N. J. Climate Change and the Precipitation Variations in the Northwestern Himalaya: 1866–2006. International Journal of Climatology, 30:535–548, 2010.

[11] Narasimha, R. and Bhattacharyya, S. A wavelet cross-spectral analysis of solar–ENSO–rainfall connections in the Indian monsoons. *Applied and Computational Harmonic Analysis*, 28:285-295, 2010.

[12] Brockwell, P. J. and Davis, R. A. *Time Series: Theory and Methods. 2nd e*dition, Springer, 1991.

[13] Bloomfield, P. *Fourier Analysis of Time Series: An Introduction*. John Wiley and Sons INC., 2nd edition, 2000.

[14] Stoica, P. and Moses, R. *Spectral analysis of signals.* Prentice Hall, Upper Saddle River, New Jersey, *07458,* 2005.

[15] Stein, J. Y. *Digital Signal Processing: A Computer Science Perspective.* John Wiley & Sons Inc., 2000.

[16] Brockwell, P. J. and Davis, R. A. *Introduction to Time Series and Forecasting.* 2nd edition; Springer, 2002.